INFLUENCE OF FATIGUE PRECRACKING ON MIXED-MODE STRESS-CORROSION CRACKING PROCESSES

J. Toribio, V. Kharin and E. Ovejero
Department of Materials Engineering, University of Salamanca
E.P.S., Campus Viriato, Avda. Requejo 33, 49022 Zamora
Tel: 980 545 000; Fax: 980 545 002, E-mail: toribio@usal.es

Abstract. This work describes experimental evidence of mixed-mode stress-corrosion cracking of high-strength steel and discusses the role of cyclic load history. To this end, finite deformation analysis of a plane strain crack subjected to mode I loading under small scale yielding was performed and different continuum mechanics variables were analysed, in particular the equivalent plastic strain, the hydrostatic stress and the plastic strain rate. Results of the computational elastoplastic demonstrate that the maximum values of the analysed variables are achieved outside the symmetry plane, which is consistent with the experimental fact of anisotropic cracking behaviour of prestressing steel in corrosive environment (in conditions of hydrogen assisted cracking and localised anodic dissolution). It can explain –if coupled with the inherent anisotropy associated with the oriented microstructure of the steel– why crack branching takes place at a deflection angle of 80º in relation to mode I crack extension.

Resumen. Este artículo describe evidencias experimentales de corrosión bajo tensión en modo mixto en aceros de alta resistencia y analiza el papel de la historia previa de carga sobre la muestra en la iniciación de dicho fenómeno. A tal efecto se realizó un análisis numérico –mediante el método de los elementos finitos en régimen elastoplástico y grandes deformaciones– del papel de la prefisuración por fatiga y su influencia sobre el campo tenso-deformacional próximo al extremo de la fisura, estudiando en particular la deformación plástica equivalente, la tensión hidrostática y la velocidad de deformación plástica. Los resultados del cálculo numérico demuestran que los valores máximos de las variables de análisis se encuentran fuera del plano de simetría, lo que resulta consistente con el hecho experimental del comportamiento anisótropo del acero en lo que se refiere a fractura en ambiente agresivo (en condiciones de fisuración asistida por hidrógeno y disolución anódica localizada) . Esto permite explicar –junto con la anisotropía resistente inherente al propio material– por qué se produce la ramificación de la fisura con un ángulo de desviación de unos 80º con respecto a la dirección original de propagación en modo I.

1. INTRODUCTION

Fatigue pre-cracking is a very common and useful crack generating technique for posterior stress corrosion testing. However, it has been documented many times that fatigue pre-loading substantially alters the results from stress-corrosion cracking tests in different aggressive environments (cf. [1,2]), so that the role of cyclic pre-loading in environmentally assisted fracture is far from being totally understood.

This work describes experimental evidence of mixed-mode stress-corrosion cracking of high-strength cold drawn steel and discusses the role of cyclic load history, in addition to the inherent strength anisotropy of the material as a consequence of the oriented pearlitic microstructure after the steelmaking process by means of very heavy drawing [3,4].

2. EXPERIMENTAL PROCEDURE

The material used is a cold drawn prestressing steel wire whose chemical composition and mechanical properties are given in Tables 1 and 2. Metallographic techniques [5,6], were used to reveal the pearlitic microstructure of the steel. Figs. 1 and 2 show micrographs of the two basic microstructural levels of pearlitic colonies and lamellae. Both microstructural units are seen to become

markedly oriented in a direction parallel or quasi-parallel to the wire axis or cold drawing direction.

Table 1. Chemical composition (wt%) of the steel

C	Mn	Si	P	S	Cr	V	Al
0.80	0.69	0.23	0.012	0.009	0.265	0.060	0.004

Table 2. Mechanical properties of the steel

Young's modulus (GPa)	Yield strength (MPa)	UTS (MPa)	Elong. at UTS (%)	Ramberg-Osgood* P (MPa)	n
199	1500	1760	5.0	2340	11.49

* Ramberg-Osgood stress-strain curve $\varepsilon = \sigma/E + (\sigma/P)^n$

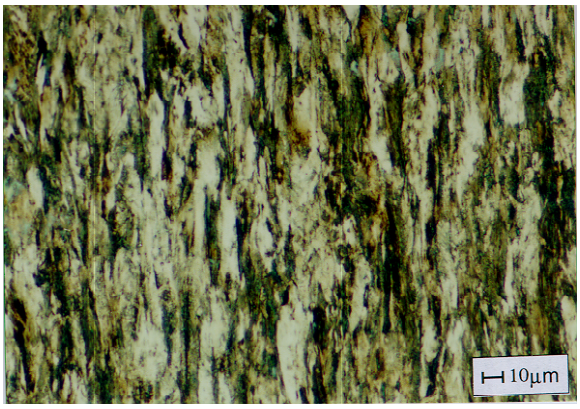


Fig. 1. Optical micrograph of the longitudinal metallographic section showing the first microstructural level: the pearlite colonies oriented after cold drawing (vertical side: wire axis or cold drawing direction).



Fig. 2. SEM micrograph of the longitudinal metallographic section showing the 2nd microstructural level: the pearlitic lamellae oriented after cold drawing (vertical side: wire axis or cold drawing direction).

Slow strain rate tests were performed on transversely precracked rods immersed in aqueous environment. Specimens were precracked by axial fatigue in air with a maximum cyclic stress intensity factor at the final phase $K_{max} = 0.30K_{IC}$, $K_{IC} = 107$ MPam$^{1/2}$ being the fracture toughness. An aqueous solution of 1 g/l $Ca(OH)_2$ + 0.1 g/l NaCl (pH=12.5) was used. Tests were conducted at a crosshead speed of $1.7x10^{-3}$ mm/min using two constant electrochemical potentials E = –1200 mV SCE (cathodic) and E = –600 mV SCE (anodic). In the former the environmental mechanism *is hydrogen assisted cracking* (HAC) whereas in the second it is *localised anodic dissolution* (LAD) [1,7].

The main phenomenological result of HAC tests is the special *fracture profile* (Fig. 3), with an angle of about 80º between the plane of the fatigue precrack (in mode I) and the direction of hydrogen-assisted initiation and crack growth. Therefore, *mixed-mode hydrogen-assisted cracking* takes place from the very initiation —just at the tip of the fatigue precrack— with no propagation in mode I in the hydrogen environment. From the fractographic viewpoint, the mixed mode propagation exhibits a hydrogen damage topography with evidence of ductile tearing (Fig. 4). It can be viewed as a typical *tearing topography surface* or TTS [8-10] altered by shear along the deviated crack plane.

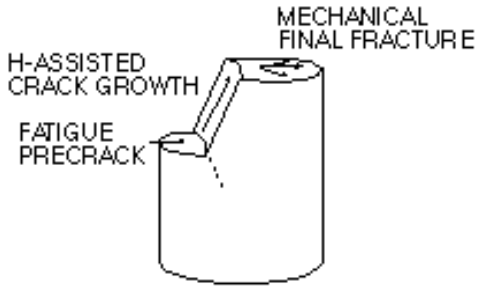


Fig. 3. Aspect of the fracture profile in the HAC test showing *early* mixed-mode propagation just after the fatigue precrack.

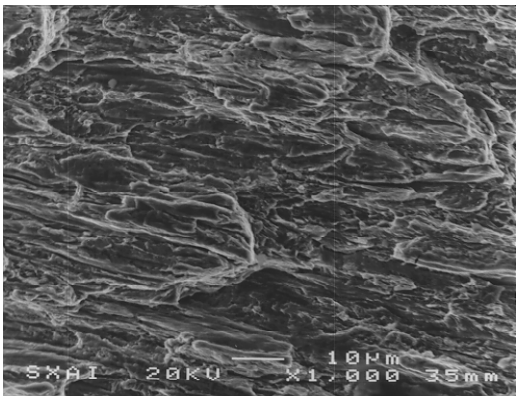


Fig. 4. Scanning electron micrograph of the mixed-mode hydrogen-assisted crack growth path, showing hydrogen damage topography with evidence of shear (crack growth from left to right).

In the LAD tests there is again a special *fracture profile* (Fig. 5) associated with the anisotropic behaviour of the cold drawn steel wire. Cracking from the tip of the mode I fatigue pre-crack develops initially in mode I and later at an angle about 75º to its plane, thus producing mixed mode propagation.

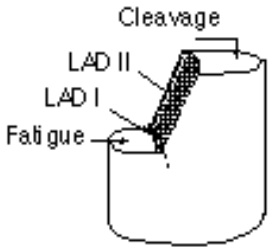


Fig. 5. Aspect of the fracture profile in the LAD test showing subcritical (slow) crack growth by localized anodic dissolution in mode I (LAD I) and mixed-mode with a strong mode II component (LAD II).

After the fractographic analysis, Fig. 6 shows the microscopic fracture modes associated with the subcritical crack growth area LAD I (before crack branching). The general appearance of the topography LAD I is similar to the micro-void coalescence (MVC) fracture mode in the same steel in air, although the former is produced by metal dissolution.

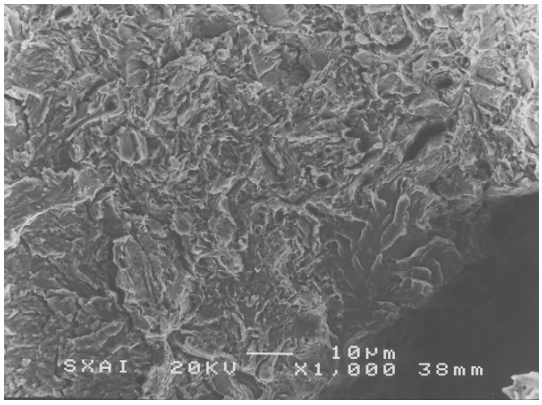


Fig. 6: Scanning electron micrograph of the subcritical crack growth area LAD I (before crack branching).

Figs. 7 shows the microscopic fracture modes associated with the subcritical crack growth area LAD II (after crack deflection). As in the previous case, this topography is also similar to MVC, although in this case there is a kind of *enlargement* or *orientation* of the micro-fracture units along the propagation direction which is quasi-parallel to the cold drawing axis (after crack deflection). Fig. 8 shows the microscopic appearance of the crack branching area, i.e., the separation (discontinuity) between the two zones LAD I and LAD II. Some cleavage facets may be observed near such a separation, which indicates that fast fracture is locally produced at the moment of crack branching, probably because the macroscopic crack reaches a point with local pre-damage produced by cold drawing.

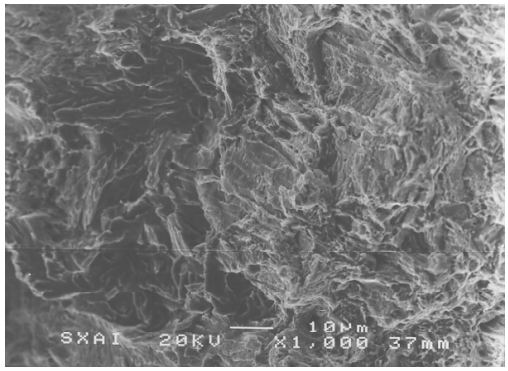


Fig. 7. SEM micrograph of the subcritical crack growth area LAD II (after crack deflection).

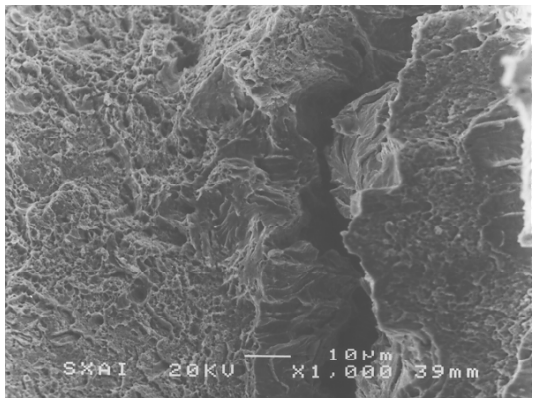


Fig. 8. SEM micrograph of the crack branching area, i.e., the separation (discontinuity) between the two zones LAD I and LAD II, showing some cleavage facets near such a separation.

The primary reason for this crack deviation is the very oriented pearlitic microstructure of the steel (cf. [11,12]) producing strength anisotropy. However, fatigue pre-cracking could be an additional factor contributing to crack deflection due to the special distribution of variables (stresses and strains) in the vicinity of a crack tip subjected to repetitive cyclic loading, as discussed in the following section of the paper devoted to the numerical modelling of the stress-strain histrory in the vicinity of the crack tip.

3. NUMERICAL MODELLING

In this paper the effect of fatigue precracking is analysed by numerical modelling of the stress-strain state near the crack tip under plane-strain small-scale yielding in an elastoplastic material with kinematic strain-hardening whose characteristics correspond to the steel used in the experimental programme (cf. Table 2). The crack was

modelled as a round-tip slit with initial height (twice the tip radius) of 2.5 μm in agreement with experimental data for fatigue cracks in high-strength steels [13]. The loading history consisted of several (up to ten) zero-to-tension cycles according to the final phase of the experimental fatigue precracking programme with K_{max}= 32 MPam$^{1/2}$ (0.30K_{IC}) followed by rising load to reproduce the slow strain rate testing. The nonlinear finite element code MARC [14] was employed with updated Lagrangian formulation.

Attention was paid to the patterns of evolution of the following continuum mechanics variables:

(i) *Equivalent plastic strain* as a measure of mechanical pre-damage [15] previous to HAC. In the case of LAD, it produces a more disordered material structure therein before stress corrosion cracking and enhances posterior dissolution in the near-tip area. In a coupled way, it has been shown that local anodic dissolution enhances crack tip deformation [16-19].

(ii) *Equivalent plastic strain rate* responsible for the dynamic phenomenon of passive film rupture due to the deformation itself. In addition, this variable also governs hydrogen transport by moving dislocations in the plastic zone [20,21] and it is known [22,23] that, even at anodic potentials, hydrogen may be present in the critical area as a consequence of the very *local* electrochemical conditions near the crack tip.

(iii) *Hydrostatic stress* as the macroscopic variable governing hydrogen transport by a mechanism of random-walk stress-assisted diffusion [24,25], according to which hydrogen (present in the near-tip area due to the local electrochemical conditions) diffuses towards the points of maximum hydrostatic stress, so that it is driven by the *gradient* of this variable.

The listed governing variables were studied at monotonic rising loading after fatigue to reproduce the slow strain rate tests. However, in some cases there is a certain subcritical crack growth in mode I before crack deflection. This means that the numerical analysis of the variables gives the stress-strain state in the vicinity of the deformed crack tip *without* considering subcritical crack extension by stress corrosion cracking, i.e., neglecting the stress-strain redistribution as a consequence of the crack growth in mode I.

4. DISCUSSION

The distribution of equivalent plastic strain at a reference stress intensity factor K_r = 0.44 K_{IC} > K_{max} (K_{max} is the maximum during the last stage of fatigue precracking) is given in Fig. 9 in the deformed configuration of the near-tip domain (the crack plane being the *x*-axis and the load applied in the *y*-direction). A vertex is observed on the tip profile with secondary peaks of equivalent plastic strain out of the crack plane. Two localized shear bands emerge from the vertex, one of them very close to the drawing direction and markedly deviated from the precrack line. The formation of this band as the easier fracture path, together with the strength anisotropy of the oriented microstructure (weakness in the wire axis or cold drawing direction), is consistent with crack kinking in the stress corrosion cracking tests (Figs. 3 and 5).

Fig. 10 displays the distribution of equivalent plastic strain rate for rising load after precracking (at K_r = 0.44 K_{IC} > K_{max}). One of the bands of fast plastic straining (and associated passive film rupture and dislocation motion) is approximately located along an 80º-direction from the initial crack plane. This indicates the preferred direction of film rupture and further localised anodic dissolution along the newly created fresh surface. This 80º-direction also signals the preferred path for hydrogen transport by dislocational dragging as the plastic zone spreads. This fact, in addition to the weakening in this direction produced by microstructural orientation, is another reason for crack deflection in agreement with the experimental cracking profile shown in Figs. 3 and 5.

Fig. 11 shows the distribution of hydrostatic stress for rising loading after fatigue cycling (at K_r = 0.44 K_{IC} > K_{max}). The closeness of the iso-lines suggests that the maximum hydrostatic stress gradient which drives stress-assisted hydrogen diffusion is achieved outside the initial crack plane. The ridge of the relief of hydrostatic stress follows a direction of 45 to 80º to the mode I plane and this indicates the area of fastest hydrogen accumulation. Hydrogen is driven in the directions of the arrows (elevated hydrostatic stress gradients and accelerated hydrogen flux) rather than ahead of the crack tip (along *x*-axis) where the flux is even delayed by the local drop of hydrostatic stress. This facilitates crack deflection and is consistent with the experienced HAC and LAD paths shown in Figs. 3 and 5.

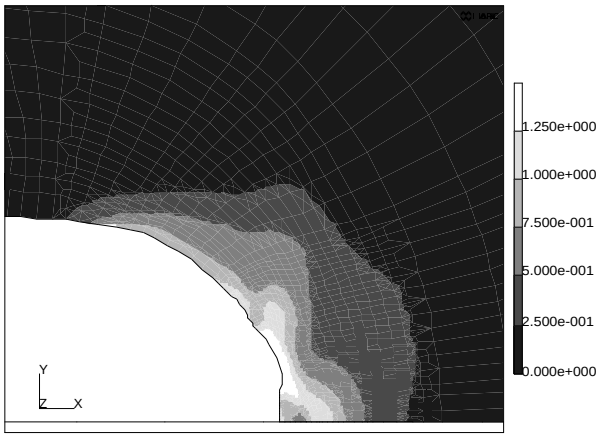


Figure 9. Distribution of equivalent plastic strain (arbitrary units) near the deformed crack tip at K_r = 0.44 K_{IC} in a slow strain rate test after fatigue cycling with K_{max} = 0.30 K_{IC}.

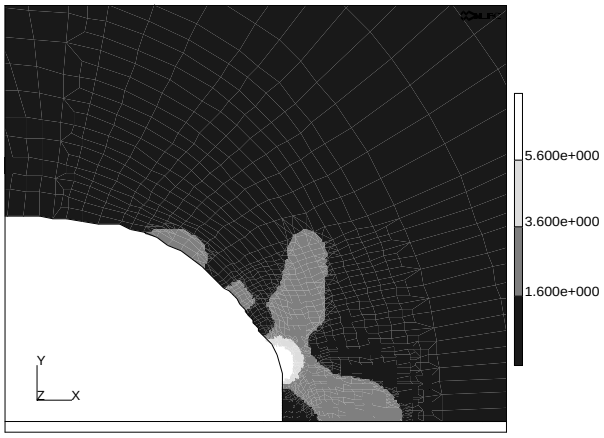


Fig. 10. Distribution of equivalent plastic strain rate (arbitrary units) near the deformed crack tip at K_r = 0.44 K_{IC} in a slow strain rate test after fatigue cycling with K_{max} = 0.30 K_{IC}.

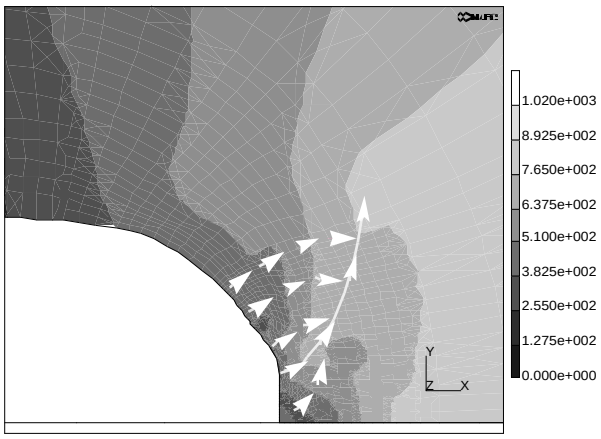


Fig. 11. Distribution of hydrostatic stress (arbitrary units) near the deformed crack tip at K_r = 0.44 K_{IC} in a slow strain rate test after fatigue cycling with K_{max} = 0.30 K_{IC}; bold line shows the ridge of the hydrostatic stress relief and arrows mark hydrostatic stress gradients and corresponding directions of accelerated hydrogen flux near the crack tip.

5. CONCLUSION

Results of the computational elastoplastic analysis are consistent with the experimental fact of anisotropic stress-corrosion cracking behaviour of prestressing steel. This explains, in addition to the inherent anisotropy associated with the oriented microstructure of the steel, why crack branching takes place in the case of hydrogen assisted cracking and localised anodic dissolution.

REFERENCES

[1] Toribio, J., Lancha, A.M. and Elices, M. (1993) *Corros. Sci.* **35**, 521.

[2] Toribio, J. and Kharin, V. (1997) *Mater. & Design* **18**, 87.

[3] Langford, G. (1970) *Metall. Trans.* **1**, 465.

[4] Embury, J.D. and Fisher, R.M. (1966) *Acta Metall.* **14**, 147.

[5] Samuels, L.E. (1992). *Optical Microscopy of Carbon Steels*, ASM, Metals Park, Ohio.

[6] Vander Voort, G.F. (1984). *Metallography. Principles and Practice*, McGraw-Hill Inc., New York.

[7] Parkins, R.N., Elices, M., Sánchez-Gálvez, V. and Caballero, L. (1982) *Corros. Sci.* **22**, 379.

[8] Thompson, A. W. and Chesnutt, J.C. (1979). *Metall. Trans*. **10A**, 1193.

[9] Costa, J.E. and Thompson, A.W. (1982*). Metall. Trans*. **13A**, 1315.

[10] Toribio, J., Lancha, A.M. and Elices, M. (1992) *Metall. Trans* **23A**, 1573.

[11] Toribio, J. and Ovejero, E. (1998*). J. Mater. Sci. Lett*. **17**, 1037.

[12] Toribio, J. and Ovejero, E. (1998*). Mech. Time-Dependent Mater.* **1**, 307.

[13] Handerhan, K.J. and Garrison Jr., W.M. (1992) *Acta Metall. Mater.* **40**, 1337.

[14] MARC User Information (1994). Marc Analysis Research Corporation, Palo Alto.

[15] Suresh, S. (1991). *Fatigue of Materials*, Cambridge University Press, Cambridge.

[16] Revie, R.W. and Uhlig, H.H. (1972) *Corros. Sci.* **12**, 669.

[17] Kramer, I.R. (1974) *Scripta Metall.* **8**, 1231.

[18] Uhlig, H.H. (1981) *Corros. Sci.* **21**, 159.

[19] Wei, X., Li, J., Zhou, X. and Ke, W. (1996) *Corros. Sci.* **38**, 989.

[20] Tien, J.K., Thompson, A.W., Bernstein, I.M. and Richards, R.J. (1976) *Metall. Trans.* **7A**, 821.

[21] Nair, S.V., Jensen, R.R. and Tien, J.K. (1983) *Metall. Trans.* **14A**, 385.

[22] Barth, C.F., Steigerwald, E.A. and Troiano, A.R. (1969) *Corrosion-NACE* **25**, 353.

[23] Smith, J.A., Peterson, M.H. and Brown, B.F. (1970) *Corrosion-NACE* **26**, 539.

[24] Van Leeuwen, H.P. (1974) *Engng. Fracture Mech.* **6**, 141.

[25] Toribio, J. and Kharin, V. (1997) *Fatigue Fracture Engng. Mater. Structures* **20**, 729.